

We are IntechOpen, the world's leading publisher of Open Access books Built by scientists, for scientists

6,900

Open access books available

186,000

International authors and editors

200M

Downloads

Our authors are among the

154

Countries delivered to

TOP 1%

most cited scientists

12.2%

Contributors from top 500 universities



WEB OF SCIENCE™

Selection of our books indexed in the Book Citation Index
in Web of Science™ Core Collection (BKCI)

Interested in publishing with us?
Contact book.department@intechopen.com

Numbers displayed above are based on latest data collected.
For more information visit www.intechopen.com



Modelling of Fracture of Anisotropic Composite Materials Under Dynamic Loads

Andrey Radchenko and Pavel Radchenko

Additional information is available at the end of the chapter

<http://dx.doi.org/10.5772/48549>

1. Introduction

At present, the wide application of the materials with preset directivity of properties in various fields of engineering defines the increased interest to the investigations of anisotropic materials behaviour under various conditions. But in Russia as well as abroad such investigations are conducted mainly for static conditions. The behaviour of anisotropic materials under dynamic loads is practically not investigated. This is especially the case with experimental investigations as well as with mathematical and numerical modelling. The impact interaction of the solids in a wide range of kinematic and geometric conditions is the complex problem of mechanics. The difficulties, connected with the theoretic study of the fracture and deformation of materials on impact by analytical methods force to introduce member of simplifying hypothesis which distort the real picture in majority of cases. In this connection it should be accepted that the leading role in the investigation of phenomena, connected with high-speed interaction of solids belongs to the experimental and numeric investigations at present. The investigations of the material damage under impact show that the fracture mechanisms change with the interaction conditions. The experiments strongly testifiers that in a number of case the resulting fracture is determined by the combination of several mechanisms. But in the experiments we fail to trace sequence, operation time and the contribution of various fracture mechanisms. Besides, the distractions, obtained at the initial stages of the process can't always be identified in the analysis of the resulting fracture of the materials. For anisotropic materials the strength itself is multivalued and uncertain notion due to the polymorphism of behaviour of these materials under the load. The limiting state of anisotropic bodies may be of different physical nature in dependence on load orientation, stressed state type and other factors. The dependence of the physical nature of limiting states is revealed in the sturdy of the experimental data. The investigations of hydrostatic pressure effect upon the strength of isotropic materials show that comprehensively the compression exerts a weak action on the

resistance of isotropic materials under static loads. Therefore, the classic theories of strength, plasticity and creep are based on assumption about the lack of the effect of fall stress tensor upon strength isotropic materials. In the experiments with anisotropic materials it was state that flow phenomenon may arise only under the action of hydrostatic pressure. Upon the materials, strength is due to the anisotropy. The shape of anisotropic bodies changes under the action of hydrostatic pressure. If these changes reach such values that, they don't disappear under relief, the limiting state should come. Therefore, the postulate of classic strength that hydrostatic pressure can't transfer the material to the dangerous state is not valid for anisotropic materials. The phenomenological approach to the investigation of the dynamics of deformation and fracture of anisotropic and isotropic materials is used in the project. The phenomenological approach to the materials strength requires that the conditions of the transition into the limiting state of various physical natures should be determinated by one equation (criterion). The necessity of such an approach results from fracture polymorphism, being deduced experimentally. For anisotropic bodies the phenomenological approach has many advantages, since there appears the possibility to use general condition of strength for the material different in composition and technology but similar in symmetry of properties, and also for the materials with substantial anisotropy, for which one and the same stressed state can result in limiting conditions, different in physical nature.

2. Equations of the model

2.1. Basic equations

The system of the equations describing non-stationary adiabatic movements of the compressed media in the Cartesian coordinate system XYZ , includes following equations (Johnson, 1977):

- continuity equation

$$\dot{\rho} + \text{div } \rho \vec{v} = 0 \quad (1)$$

- motion equation

$$\begin{aligned} \rho \dot{u} &= \sigma_{xx,x} + \sigma_{xy,y} + \sigma_{xz,z} \\ \rho \dot{v} &= \sigma_{yx,x} + \sigma_{yy,y} + \sigma_{yz,z} \\ \rho \dot{w} &= \sigma_{zx,x} + \sigma_{zy,y} + \sigma_{zz,z} \end{aligned} \quad (2)$$

- energy equation

$$\dot{E} = \frac{1}{\rho} \sigma_{ij} e_{ij}; \quad i, j = x, y, z \quad (3)$$

Here ρ – density of media; \vec{v} – velocity vector, u, v, w – components of velocity vector on axes x, y, z accordingly; σ_{ij} – components of a symmetric stress tensor; E – specific

internal energy; e_{ij} – components of a symmetric strain rate tensor; the point over a symbol means a time derivative; a comma after a symbol – a derivative on corresponding coordinate.

The behavior of the aluminum isotropic cylinder at high-velocity impact is described by elastic-plastic media, in which communication between components of strain velocity tensor and components of stress deviator are defined by Prandtl-Reuss equation:

$$2G \left(e_{ij} - \frac{1}{3} e_{kk} \delta_{ij} \right) = \frac{DS^{ij}}{Dt} + \lambda S^{ij}, \quad (\lambda \geq 0); \quad \frac{DS^{ij}}{Dt} = \frac{dS^{ij}}{dt} - S^{ik} \omega_{jk} - S^{jk} \omega_{ik} \quad (4)$$

where $\omega_{ij} = \frac{1}{2} (\nabla_i v_j - \nabla_j v_i)$, G – shear modulus. Parameter $\lambda = 0$ at elastic deformation, and at elastic ($\lambda > 0$) is defined by means of a Mises condition:

$$S^{ij} S_{ij} = \frac{2}{3} \sigma_d^2 \quad (5)$$

where σ_d – dynamic yield point. The ball part of stress tensor (pressure) is calculated on the Mi-Gruneisen equation as function of specific internal energy E and density ρ :

$$P = \sum_{n=1}^3 K_n \left(\frac{V_0}{V} - 1 \right)^n \left[\frac{1 - K_0 \left(\frac{V_0}{V} - 1 \right)}{2} \right] + K_0 \rho E \quad (6)$$

where K_0, K_1, K_2, K_3 – constants of material.

2.2. Model of deformation and fracture of anisotropic materials

The behavior of an anisotropic material of targets is described within the limits of elastic-fragile model. Before fracture components of a stress tensor in a target material were defined from equations of the generalized Hooke's law which have been written down in terms of strain rate:

$$\dot{\sigma}_{ij} = C_{ijkl} e_{kl} \quad (7)$$

where C_{ijkl} – elastic constants.

Thus components of a tensor of elastic constants possess, owing to symmetry of stress tensors and strain tensors and presence of the elastic potential, following properties of symmetry:

$$C_{ijkl} = C_{jikl} = C_{ijlk} = C_{jilk}; \quad C_{ijkl} = C_{klij} \quad (8)$$

At transition to another, also orthogonal, coordinate system, elastic constants will be transformed by equations:

$$C'_{abcd} = C_{ijkl} q_{ia} q_{jb} q_{kc} q_{ld} \quad (9)$$

where q_{ij} – cosine of the angle between corresponding axes i and j . In three-dimensional space transformation of the component of a tensor of the fourth rank demands summation of the compositions, containing as multipliers 4 cosines of angles of rotation of axes.

Fracture of an anisotropic material is described within the limits of model with use of Tsai-Wu fracture criterion with various ultimate strengths of pressure and tension (Tsai & Wu, 1971). This criterion, which has been written down by scalar functions from components of a stress tensor, has the following appearance:

$$f(\sigma_{ij}) = F_{ij} \sigma_{ij} + F_{ijkl} \sigma_{ij} \sigma_{kl} + \dots \geq 1; \quad i, j, k, l = 1, 2, 3 \quad (10)$$

Here F_{ij} and F_{ijkl} are components of tensor of the second and the fourth rank respectively, and obey transformation laws:

$$F'_{ab} = F_{ij} q_{ia} q_{jb}; \quad F'_{abcd} = F_{ijkl} q_{ia} q_{jb} q_{kc} q_{ld} \quad (11)$$

Components of tensors of strength for criterion are defined by following equations:

$$F_{ii} = \frac{1}{X_{ii}} - \frac{1}{X'_{ii}}; \quad F_{iii} = \frac{1}{X_{ii} X'_{ii}}; \quad F_{ij} = \frac{1}{2} \left(\frac{1}{X_{ij}} - \frac{1}{X'_{ij}} \right); \quad F_{ijj} = \frac{1}{4 X_{ij} X'_{ij}}; \quad i \neq j \quad (12)$$

where X_{ii} , X'_{ii} – limits of strength on pressure and tension along the direction i ; X_{ij} , X'_{ij} – shear strength along the two opposite directions with $i \neq j$. Coefficients F_{1122} , F_{2233} , F_{3311} are defined at carrying out the experiments on biaxial tension in planes 1-2, 2-3, 1-3 accordingly. The remained coefficients are defined similarly at combined stressing in corresponding planes (Radchenko et al., 2012).

It is supposed that fracture of anisotropic materials in the conditions of intensive dynamic loads occurs as follows:

- if strength criterion is violated in the conditions of pressure ($e_{kk} \leq 0$), the material loses anisotropy of properties, and its behaviour is described by hydrodynamic model, thus the material keeps its strength only on pressure; the stress tensor becomes in this case spherical ($\sigma_{ij} = -P$);
- if the criterion is violated in the conditions of tension ($e_{kk} > 0$), the material is considered completely fractured, and components of a stress tensor are appropriate to be equal to zero ($\sigma_{ij} = 0$).

Pressure in orthotropic materials of targets is calculated by means of the equation of a condition (Kanel et al., 1996):

$$P = \left[\exp \left(4\beta \frac{V_0 - V}{V_0} \right) - 1 \right] \frac{\rho_0 \alpha^2}{4\beta} \quad (13)$$

Here ρ_0 is initial density of a material; V_0, V – relative initial and current volumes. Coefficients of the given equation are calculated from a shock adiabat: $D = \alpha + \beta u$, where $\alpha = 1400$ m/s, $\beta = 2.25$, and u – mass velocity.

2.3. Initial and boundary conditions

It is considered (fig. 1) a three-dimensional task of high-speed interaction of compact (diameter of the projectile is equal to its height) cylindrical projectile (area D_1) with one or several targets (areas D_2, D_3, D_4). In this paper we consider the materials with the following mechanical characteristics (Ashkenazi & Ganov, 1980): Steel St3 with $\rho_0 = 7850$ kg/m³, $E = 204$ GPa, $\mu = 0.3$, $G = 79$ GPa, $\sigma_{0.2} = 1.01$ GPa, $K_0 = 1.91$, $K_1 = 153$ GPa, $K_2 = 176$ GPa, $K_3 = 53.1$ GPa; aluminum with $\rho_0 = 2700$ kg/m³, $E = 70$ GPa, $\mu = 0.3$, $G = 27$ GPa, $\sigma_{0.2} = 310$ MPa, $K_0 = 2.13$, $K_1 = 74.4$ GPa, $K_2 = 53.2$ GPa, $K_3 = 30.5$ GPa; organoplastic with $\rho_0 = 1350$ kg/m³, $E_1 = 48.6$ GPa, $E_2 = 21.3$ GPa, $E_3 = 7.1$ GPa, $\mu_{12} = 0.28$, $\mu_{23} = 0.26$, $\mu_{31} = 0.037$, $G_{12} = 930$ GPa, $G_{23} = 900$ GPa, $G_{31} = 850$ GPa, $X_{11} = 2.67$ GPa, $X_{22} = 1.18$ GPa, $X_{33} = 0.395$ GPa, $X'_{11} = 0.37$ GPa, $X'_{22} = 0.5$ GPa, $X'_{33} = 1.94$ GPa, $X_{12} = 0.975$ GPa, $X_{23} = 0.8$ GPa, $X_{31} = 0.607$ GPa, $X_{11}^{(12)} = 2.3$ GPa, $X_{11}^{(31)} = 2$ GPa, $X_{22}^{(12)} = 1$ GPa, $X_{22}^{(23)} = 0.9$ GPa, $X_{33}^{(23)} = 0.35$ GPa, $X_{33}^{(31)} = 0.31$ GPa, $c_x = 6000$ m/s, $c_y = 3970$ m/s, $c_z = 2300$ m/s. The meeting corner (between a normal to a target and a longitudinal axis of the projectile) made a corner $\alpha = 0^\circ$ (normal impact).

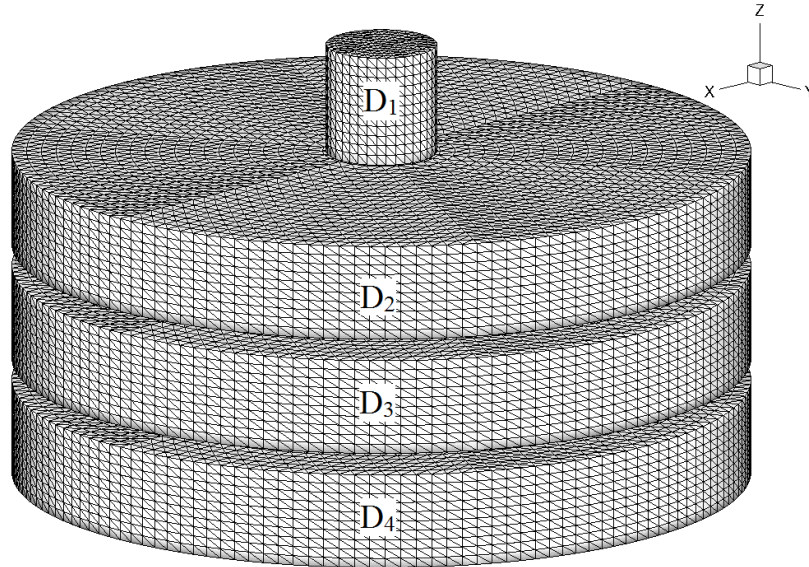


Figure 1. Three-dimensional formulation of the task

Initial conditions ($t = 0$):

$$\sigma_{ij} = E = u = v = 0, \quad w = v_0, \quad i, j = x, y, z, \quad x, y, z \in D_1 \quad (14)$$

$$\sigma_{ij} = E = u = v = w = 0, \quad i, j = x, y, z, \quad x, y, z \in D_2, D_3, D_4 \quad (15)$$

$$\rho = \rho_i, \quad x, y, z \in D_i, \quad i = 1, 2, 3, 4 \quad (16)$$

Boundary conditions:

On free surfaces conditions of free border are realized:

$$\bar{T}_{nm} = \bar{T}_{nr1} = \bar{T}_{nr2} = 0 \tag{17}$$

On contact surface sliding condition without a friction is realized:

$$\bar{T}_{nm}^+ = \bar{T}_{nm}^-, \bar{T}_{nr}^+ = \bar{T}_{nr}^- = \bar{T}_{ns}^+ = \bar{T}_{ns}^- = 0, \bar{v}_n^+ = \bar{v}_n^- \tag{18}$$

Here \bar{n} – a unit vector of a normal to a surface in a considered point, $\bar{\tau}$ and \bar{s} – unit vectors, tangents to a surface in this point, \bar{T}_n – a force vector on a platform with a normal \bar{n} , \bar{v} – a velocity vector. The subscripts at vectors \bar{T}_n and \bar{v} also mean projections on corresponding basis vectors; the badge plus "+" characterizes value of parameters in a material on the top border of a contact surface, a badge a minus "-" – on bottom.

The problem solves numerically using the finite element method in the explicit formulation by Johnson G.R. (Johnson, 1977).

3. Check of adequacy of the model

The series of test calculations for check convergence of the solution (independence of the solution from a spatial interval) has been passed. Dependence of the σ_{xx} component in the central point of a target from total number of elements N_E in a calculating grid was considered. The received curve shows fast convergence of the decision at a grid compaction (fig. 2).

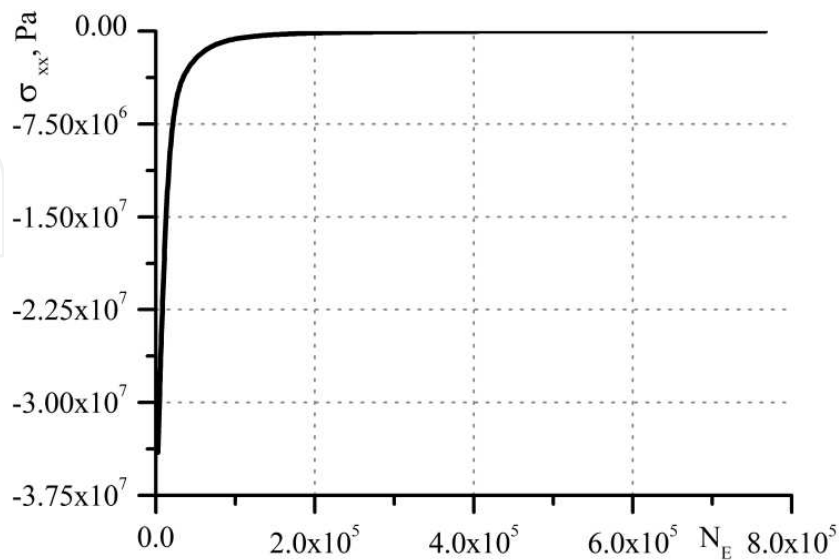


Figure 2. Convergence of the solution

3.1. Experiments with isotropic materials

In connection with a considerable quantity of works on a problem of impact on rigid target, numerical experiments for check of the numerical methods have been made. The problem about normal impact of the cylindrical projectile with length $L_0 = 23.47$ mm and diameter $D_0 = 7.62$ mm on rigid target with initial velocity v_0 is considered. Material of the projectile – steel of St3 mark. In the table 1 the received results of calculations in comparison with experiment and the data of calculations from M.L. Wilkins works on residual length of the drummer L are presented at various velocities of impact (Wilkins & Giunan, 1973). In the table 1 δ_l is the relative divergence between spent calculations and experiments.

| v_0 , m/sec | Experiment, $\frac{L}{L_0}$ | M.L. Wilkins, $\frac{L}{L_0}$ | Calculation, $\frac{L}{L_0}$ | δ_l , % |
|---------------|-----------------------------|-------------------------------|------------------------------|----------------|
| 175 | 0.911 | 0.911 | 0.915 | 0.4 |
| 252 | 0.842 | 0.842 | 0.839 | 0.4 |
| 311 | 0.766 | 0.766 | 0.760 | 0.8 |
| 402 | 0.635 | 0.667 | 0.619 | 2.5 |

Table 1. Comparison with experiments and calculations

For check of adequacy of model the number of comparisons of numerical calculations with experimental data has been spent. Table 2 shown the results of experiments and calculations at the interaction of the steel projectile with mass of 20 grams with the glass-fibre plastic isotropic targets ($\rho_0 = 1930 \text{ kg/m}^3$). The following symbols are introduced into the table: h is the target thickness, v_0 is the initial projectile velocity, v_1 is the post-perforation velocity of projectile, ε is the relative decrease of the projectile height after target piercing, δ_v is the relative divergence between post-perforation velocity of projectile in the experiment and calculation.

| h, mm | v_0 , m/sec | Experiment | Calculation | δ_v , % |
|-------|---------------|---------------|---------------|----------------|
| | | v_1 , m/sec | v_1 , m/sec | |
| 5 | 992 | 928 | 970 | 6.3 |
| 9 | 1163 | 1013 | 950 | 6.2 |
| 14 | 1064 | 812 | 780 | 4.0 |

Table 2. Comparison with experiments for isotropic targets

3.2. Experiments with anisotropic materials

A number of experiments of penetration for check of the offered model of behavior of anisotropic materials was similarly carried out (Radchenko et al., 1999). The results on beyond barrier speeds of striker at the interaction of 20-gram striker with transtropic barrier are presented in table 3.

| h, mm | v_0 , m/s | Experiment | Calculation | δ_v , % |
|-------|-------------|-------------|-------------|----------------|
| | | v_1 , m/s | v_1 , m/s | |
| 26 | 1054 | 698 | 640 | 8.3 |
| 26 | 1077 | 695 | 638 | 8.2 |
| 18 | 1012 | 897 | 836 | 6.8 |
| 18 | 956 | 838 | 792 | 5.5 |

Table 3. Comparison with experiments for anisotropic targets

Comparison of numerical and experimental results allows conclude that the proposed model satisfactorily describes the process of breaking through the isotropic and transtropic plates. A deviation of calculated values of the post-penetration velocities from the experimental values does not exceed 8.5%.

4. Deformation and fracture of anisotropic composite materials and designs under dynamic loading

4.1. Pulse effect

Problems of dynamic deformation of the ball from organoplastic under effect of omnidirectional compression pulse are considered in three-dimensional statement. Homogeneous orthotropic ball with diameter of 10 mm was subjected to compression with pulse pressure of 1 GPa during 3 μ sec (fig. 3). It is supposed that the failure of anisotropic material in condition of intense dynamic loads happens in accordance with (Radchenko et al., 1999). The material of the ball is orthotropic organoplastic. Already at the time moment of 0.6 μ sec in ZX cross section (where there is most significant difference between characteristics), the distribution of stress and field of velocities (fig. 4) illustrate the origin of heterogeneous picture of Strain-stress State of the ball. In ZY section the distribution of stress as well as field of velocities is close to one-dimension Strain-stress State of isotropic ball under the effect of omnidirectional compression (fig. 5). At this moment, the stresses achieves maximum values (-2 GPa) near at ball poles on Z axis.

In this case the ball failure arises in the region of maximum stresses. With time the Strain-stress State of anisotropic ball differs from Strain-stress State of isotropic ball more strongly. Isolines of stress and field of rates at the shown in fig. 6, fig. 7. Evident sliding lines are seen in fig. 6a and fig. 7a. Only σ_x distribution in ZY cross section (fig. 7b) is closest to the distribution of stress in isotropic ball, maximum stress are achieved in the centers.

Up to 1 μ sec in all directions, mass velocities are directed into the insight of the ball, but with of 1 μ sec, in direction X rates change the sign and the increase in ball size begins in this direction. In other directions, mass velocities are directed inside of the ball up to the moment of load removal (3 μ sec). This, maximum decrease in ball dimensions in X directions is 11% and is achieved to 1 μ sec, and in Z direction it is 24% and is achieved in 3 μ sec.

Substantial change in the shape of the ball is observed to the moment of cessation of compression pulse action (fig. 8) it acquires dump – bells shape due to the compression along Z axis.

The expansion of the ball in all directions begins after the release of the load. Fig. 9 shows the field of velocities in 6 μsec , to that moment the material of the ball has been completely fractured.

The ball under the effect of omnidirectional compression pulse may transform not to ellipsoid but to the dump – bells under the certain relations of its mechanical characteristics of the value of pressure pulse.

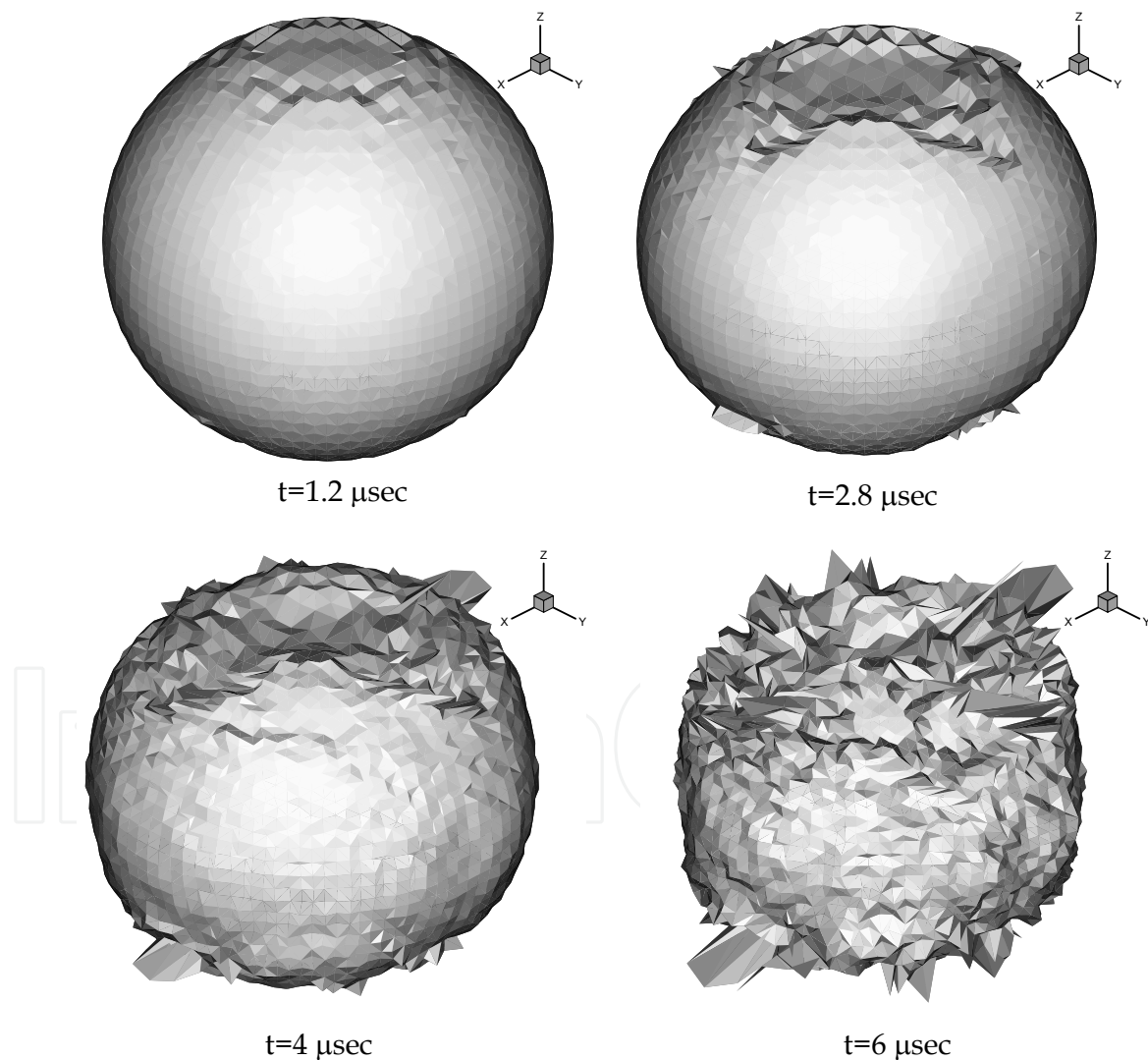


Figure 3. Volume configurations of orthotropic ball at loading by the pulse of pressure: $P = P_0$ if $t \leq \tau$ and $P = 0$ if $t > \tau$. $P = 1 \text{ GPa}$, $\tau = 3 \mu\text{sec}$

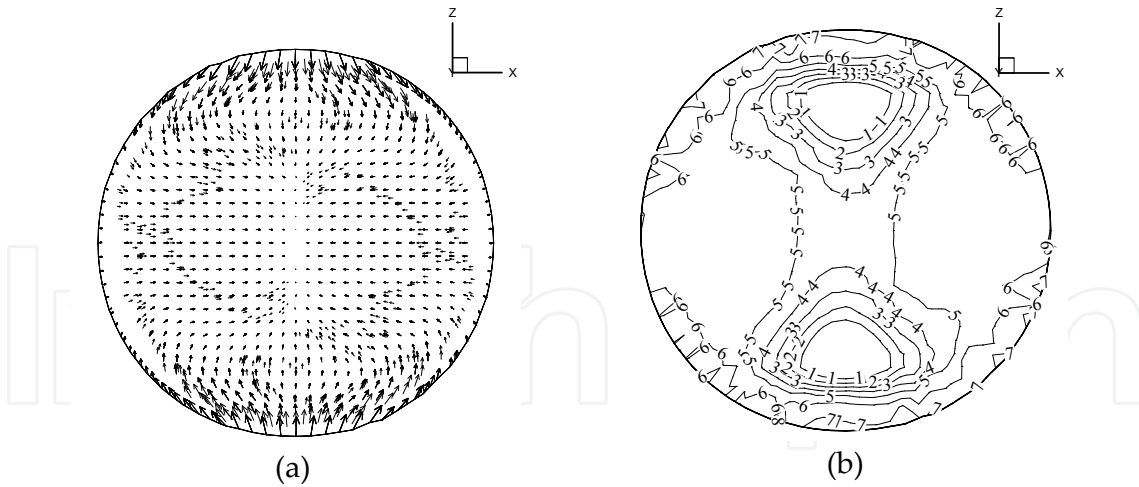


Figure 4. Field of mass velocities (a) and distribution of isolines of stress σ_x (b). $t = 0.6 \mu\text{sec}$. 1: -2, 2: -1.8, 3: -1.6, 4: -1.4, 5: -1.2, 6: -1, 7: -0.8, 8: -0.6 GPa

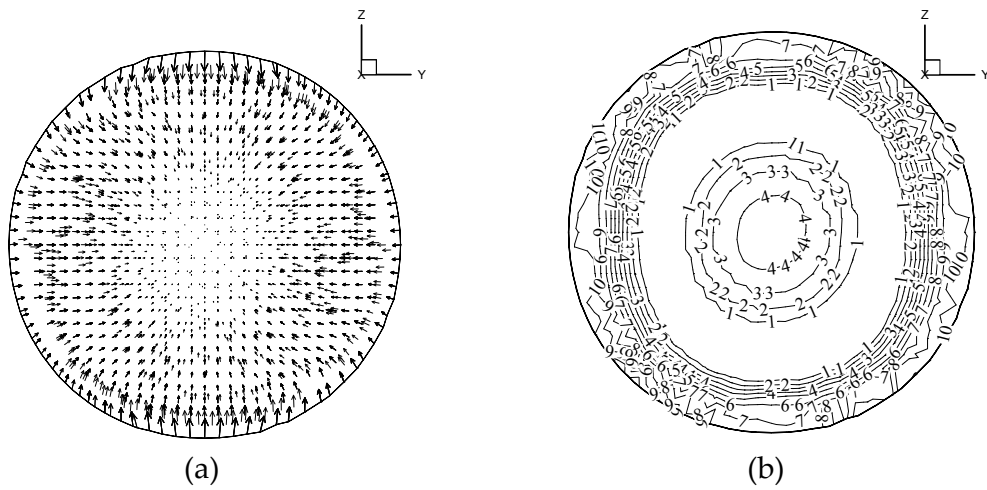


Figure 5. Field of mass velocities (a) and distribution of isolines of stress σ_x (b). $t = 0.6 \mu\text{sec}$. 1: -2, 2: -1.8, 3: -1.6, 4: -1.4, 5: -1.2, 6: -1, 7: -0.8, 8: -0.6 GPa

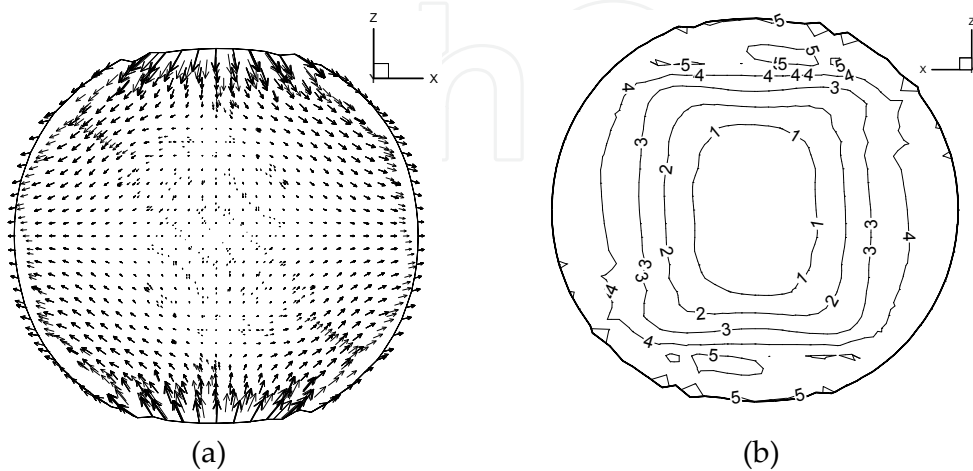


Figure 6. Field of mass velocities (a) and distribution of isolines of stress σ_x (b). $t = 1.2 \mu\text{sec}$. 1: -2.4, 2: -2, 3: -1.6, 4: -1.2, 5: -0.8, 6: -0.4, 7: 0, 8: 0.4, 9: 0.8, 10: 1.2 GPa

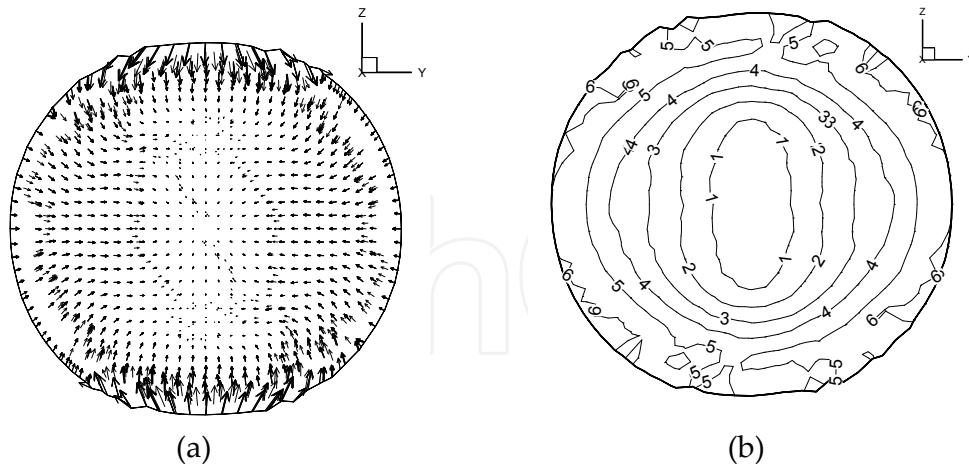


Figure 7. Field of mass velocities (a) and distribution of isolines of stress σ_x (b). $t = 1.2 \mu\text{sec}$. 1: -2.4, 2: -2, 3: -1.6, 4: -1.2, 5: -0.8, 6: -0.4, 7: 0, 8: 0.4, 9: 0.8, 10: 1.2 GPa

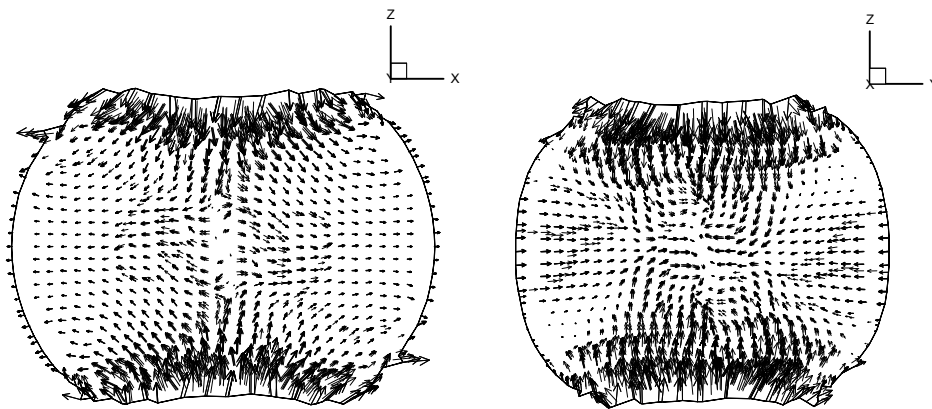


Figure 8. Field of mass velocities. $t = 3 \mu\text{sec}$.

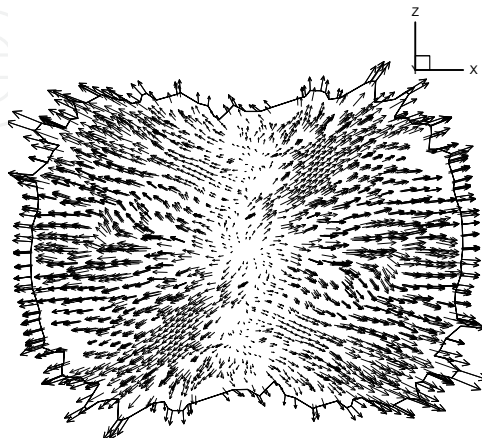


Figure 9. Field of mass velocities. $t = 6 \mu\text{sec}$.

4.2. Influence of orientation of elastic and strength properties on fracture of anisotropic materials under dynamic loading

We studied the penetration of a barrier with the initial orientation of the properties, as well as penetration of a barrier with properties reoriented by 90° about the axis OY . In the direction of the axis Z initial material has the highest strength on compression and the lowest strength on tension. Refocused the material, on the contrary, along the Z axis has the lowest compressive strength and the highest tensile strength. In addition to the various limits of the tensile and compression on the dynamics of fracture will affect significantly the velocity of propagation of waves of compression and unloading, which in an anisotropic material depend on the direction.

A material of the projectile is isotropic steel, a material of targets – orthotropic organoplastic. Orientation of properties of orthotropic material changes by turn of axes of symmetry of an initial material round an axis on an angle $\beta = 90^\circ$.

On fig. 10 and fig. 11 configurations of the projectile and targets with distribution of isolines of relative volume of fractures for various velocities of interaction at the moment of time $t = 40 \mu\text{sec}$ are presented. To the left of a symmetry axis configurations for initial orientation of a material of a target, to the right – for the reoriented material are given.

For a case of initial orientation of properties of organoplastic at velocity 50 m/s (fig. 10a, to the left of a symmetry axis) on an obverse surface of a target on perimeter of the projectile and on a contact surface in the target center the conic zones of fracture focused at an angle 45° to a direction of impact are formed. These zones arise in an initial stage of interaction at the expense of action of tensile stress in the unloading waves extending from an obverse surface of a target and a lateral surface of the projectile. The further development of these zones of fracture is caused by action of tensile stress as a result of introduction of the projectile. At initial velocity 50 m/s there is no perforation of a target. To $t = 30 \mu\text{sec}$ velocity of the projectile reduces to zero and the kickback of the projectile from a target is observed. Values of vertical component of the velocity of the center of projectile weights v_z and a part of the fractured material of a target are presented in table 4 (at tension D_t and pressure D_p at the moment of time $t = 50 \mu\text{sec}$).

| $v_0, \text{m/s}$ | 50 | | 100 | | 200 | | 400 | |
|-------------------|-----------|------------|-----------|------------|-----------|------------|-----------|------------|
| β | 0° | 90° | 0° | 90° | 0° | 90° | 0° | 90° |
| $v_z, \text{m/s}$ | -5.17 | 4.08 | 9.05 | 12.97 | 49.97 | 127.6 | 191.55 | 303.69 |
| D_t | 0.012 | 0.005 | 0.056 | 0.011 | 0.162 | 0.128 | 0.502 | 0.282 |
| D_p | 0.006 | 0.002 | 0.043 | 0.029 | 0.104 | 0.021 | 0.112 | 0.019 |

Table 4. Velocity of the center of projectile weights and part of the break material in targets

In case of the reoriented material (fig. 10a, to the right of a symmetry axis) a picture of development of fracture is qualitative other. In this case, strength of a material on pressure

in a direction of axis Z (an impact direction) is minimal. It leads to that the material break in the wave of pressure formed at the moment of impact and extending on a thickness of a target. Penetration of the projectile thus occurs in already weakened material. Though perforation in this case also isn't present, the projectile gets deeply, and its full braking is observed in $50 \mu\text{sec}$. With increase in velocity of impact the volume of areas of fracture grows. At velocity 100 m/s (fig. 10b) fracture areas extend to a greater depth on a thickness of a target. And for an initial material of a target a marked orientation (45°) was kept only by a crack extending from an obverse surface on perimeter of the projectile. The crack located near to an axis of symmetry isn't identified any more. It is caused by that with increase in velocity of impact the amplitude of the pressure wave grows – its size is already sufficient for material fracture in the top half of target.

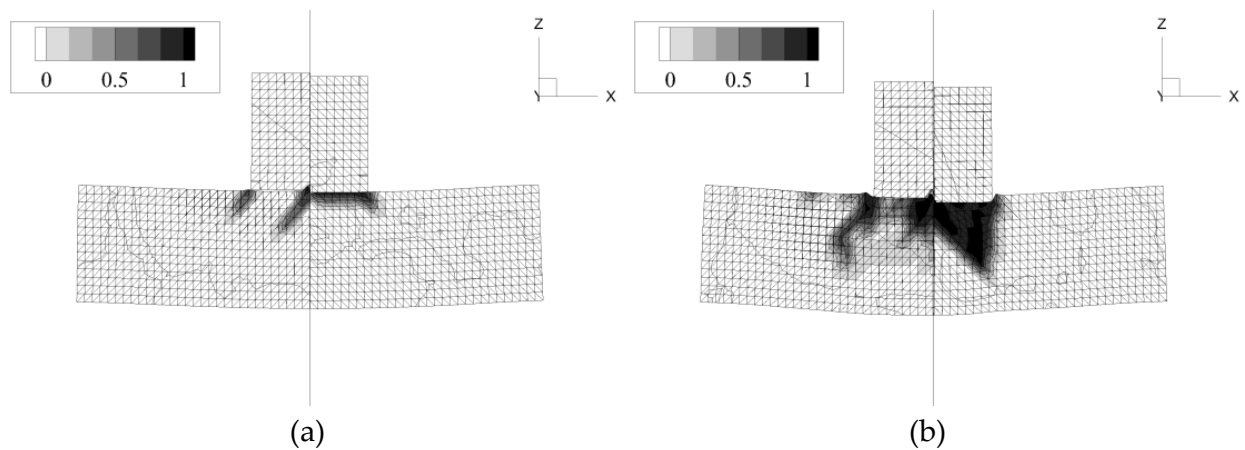


Figure 10. Relative volume of fractures in target. $v_0 = 50 \text{ m/s}$ (a) and $v_0 = 100 \text{ m/s}$ (b), $t = 40 \mu\text{sec}$.

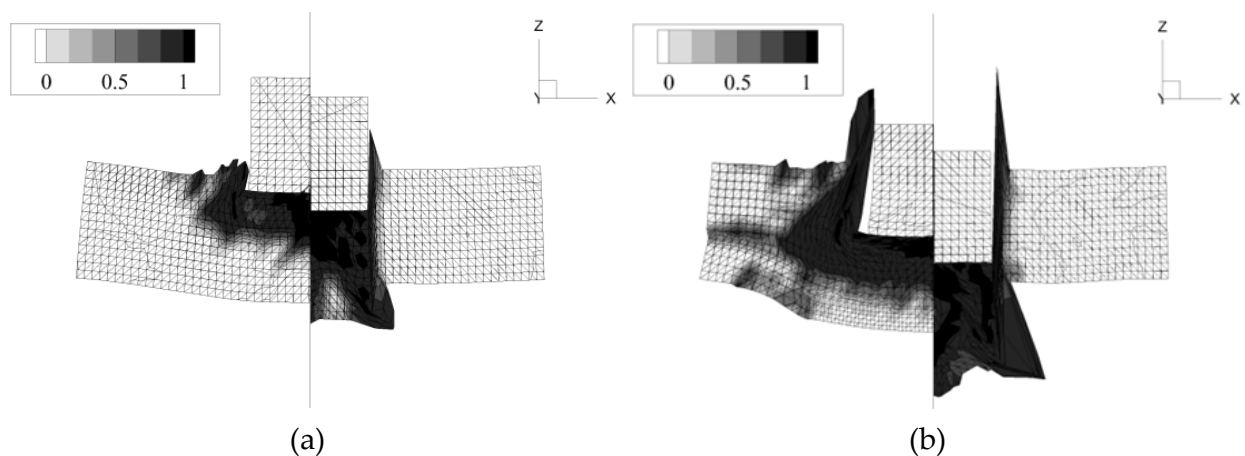


Figure 11. Relative volume of fractures in target. $v_0 = 200 \text{ m/s}$ (a) and $v_0 = 400 \text{ m/s}$ (b), $t = 40 \mu\text{sec}$.

In case of the reoriented material the unloading wave extending from a back surface of a barrier, lowers level of compressive stresses that leads to smaller distribution of fracture area on a thickness near to a symmetry axis (fig. 10b). For velocity 100 m/s also it is not observed perforation of targets, thus in case of an initial material velocity of the projectile reduced to zero at $45 \mu\text{sec}$, in case of the reoriented material – at $60 \mu\text{sec}$.

For velocities of impact 200 m/s and above (fig. 11) it is already observed perforation of targets from both types of materials. But thus the plate from an initial material greater maintains resistance to penetration of the projectile in comparison with a plate from the reoriented material. For example, at initial velocities 200 m/s (fig. 11a) and 400 m/s (fig. 11b) post-perforation velocity of the projectile after perforation of plates from an initial material makes 37 m/s and 187 m/s accordingly, and post-perforation velocity after perforation plates of the reoriented material 125 m/s and 300 m/s. Greater resistance to penetration of the projectile in plates from an initial material is caused by a various picture of fracture which is defined by orientation of elastic and strength properties in relation to external loading. For velocities of impact above 200 m/s there is fracture of the reoriented material in the unloading wave extending from a back surface of a target (fig. 11), that increases volume of the break material in front of the projectile, essentially reducing resistance to penetration. Such dynamics of fracture become clear by various velocities of wave distribution in the initial and reoriented materials.

In an initial material velocity of wave distribution the greatest in a direction of an axis X – perpendicular to an impact direction, therefore unloading waves from an obverse surface of a target and a lateral surface of the projectile lower stresses in a pressure wave to its exit on a back surface that doesn't lead to material fracture in a pressure wave in the bottom half of plate and a unloading wave from a back surface of the barrier having small amplitude at the expense of easing of a pressure wave.

In the reoriented material velocity of distribution of waves is maximal in a direction of axis Z , therefore the pressure wave loses energy only on fracture of a material and being reflected from a back surface by an intensive unloading wave breaking a material.

4.3. Numerical modeling of deformation and fracture of the composite spaced targets under impact

This paper presents a comparative analysis of fracture in monolithic and spaced barriers during high-velocity interaction with compact projectiles. The material of barriers is orthotropic organoplastic with a high degree of anisotropy of elastic and strength properties. We investigate the fracture efficiency of the protective properties of monolithic and spaced barriers depending on the orientation of anisotropic material properties in a range of velocities of impact from 750 to 3000 m/s.

At high-velocity impact on spaced designs the defining role in the fracture of the projectile and barriers is played by shock wave processes. As a result of the extension of these processes there is a fracture of the projectile and thin screens protecting the main design. Thin screens are effective for protection of space vehicles against particles of small space debris, moving at velocities more than 3 km/s at which intensive fracture of particles begins. At interaction with more massive particles with velocities not over 3 km/s thin screens are not so effective. In space similar situations are possible at the interaction of devices with space debris on catching up courses. At velocities of impact in a range not over 3 km/s an important role belongs to the strength characteristics of materials. Earlier conducted

researches of the fracture of the spaced barriers made from isotropic metal materials have shown that their efficiency, in comparison with efficiency of the monolithic barrier, increases with increase in velocity of interaction. Now for manufacturing of aircrafts elements the various types of composite materials having a high degree of anisotropy of the elastic and strength properties are used, and without such property as anisotropy it is impossible to describe and predict the behavior of design elements and of the design as a whole (Radchenko & Radchenko, 2011).

On fig. 12, 13 computational configurations of the aluminum projectile, of the monolithic barrier and also of the two-layer and three-layer spaced barriers made from anisotropic organoplastic for velocities of impact from 750 to 2000 m/s accordingly are presented.

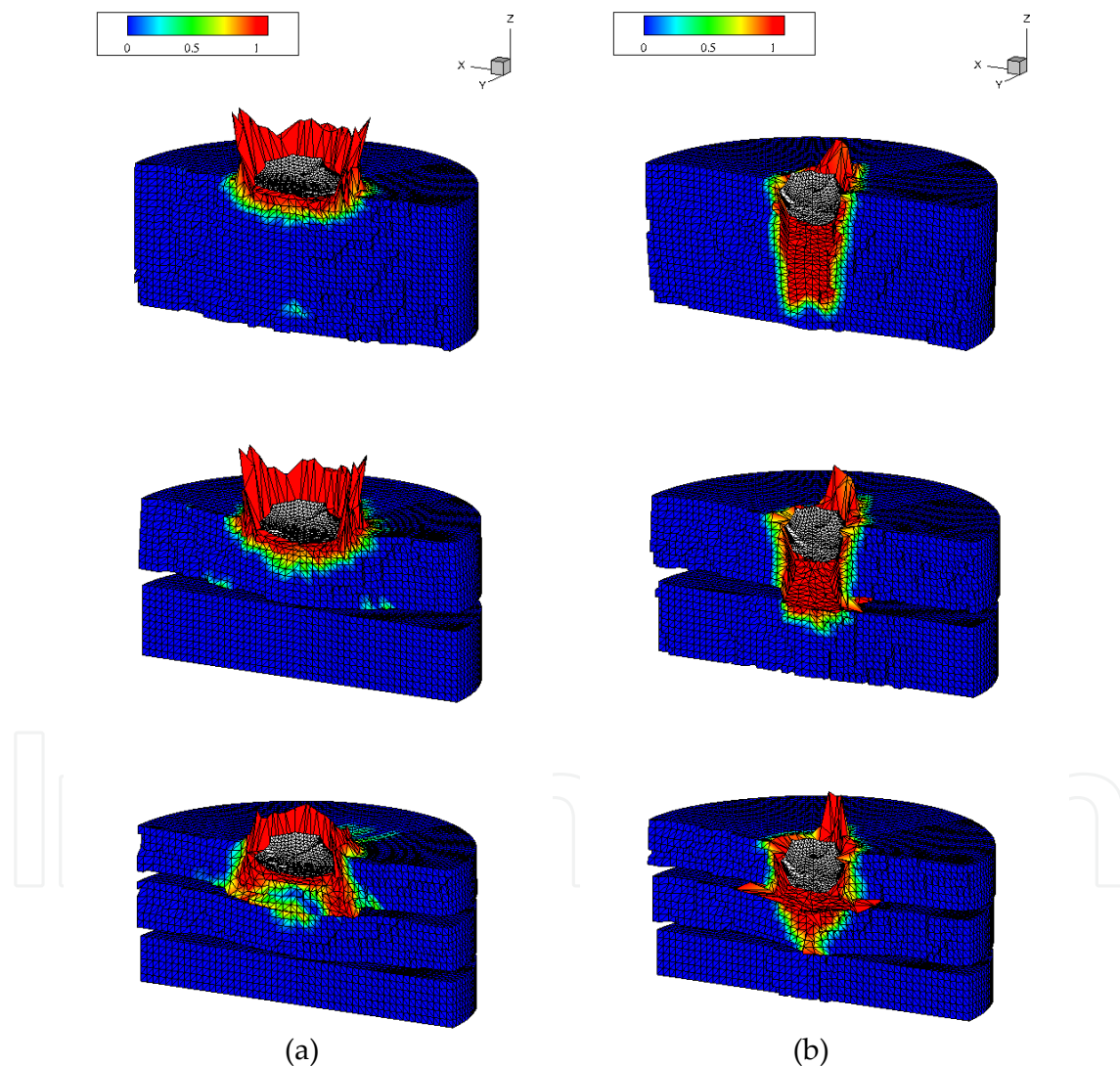


Figure 12. Calculated configurations of cooperating bodies and isolines of relative volume of fractures (V/V_0) in targets. a: $v_0 = 750$ m/s, $\beta = 0^\circ$, b: $v_0 = 750$ m/s, $\beta = 90^\circ$; $t = 40$ μ sec

On fig. 12a, fig. 13b barriers made from an initial material are given, on a fig. 12b, fig. 13b there are barriers made from reoriented material. It is necessary to explain that values of V

and V_0 are given in node of a mesh: V is a volume of incorporating elements of node in which the fracture condition was satisfied; V_0 is the total volume of the elements containing this node. Value of 1 for V/V_0 corresponds to the full fracture of the material in node of a mesh. As researches showed (Radchenko et al., 1999), a picture of the fracture observing in barriers depends on orientation of a material properties in relation to the direction of action of external loading, in this case to an impact direction. As a result the dynamic nature of fractures in a barrier defines an efficiency of its protective properties.

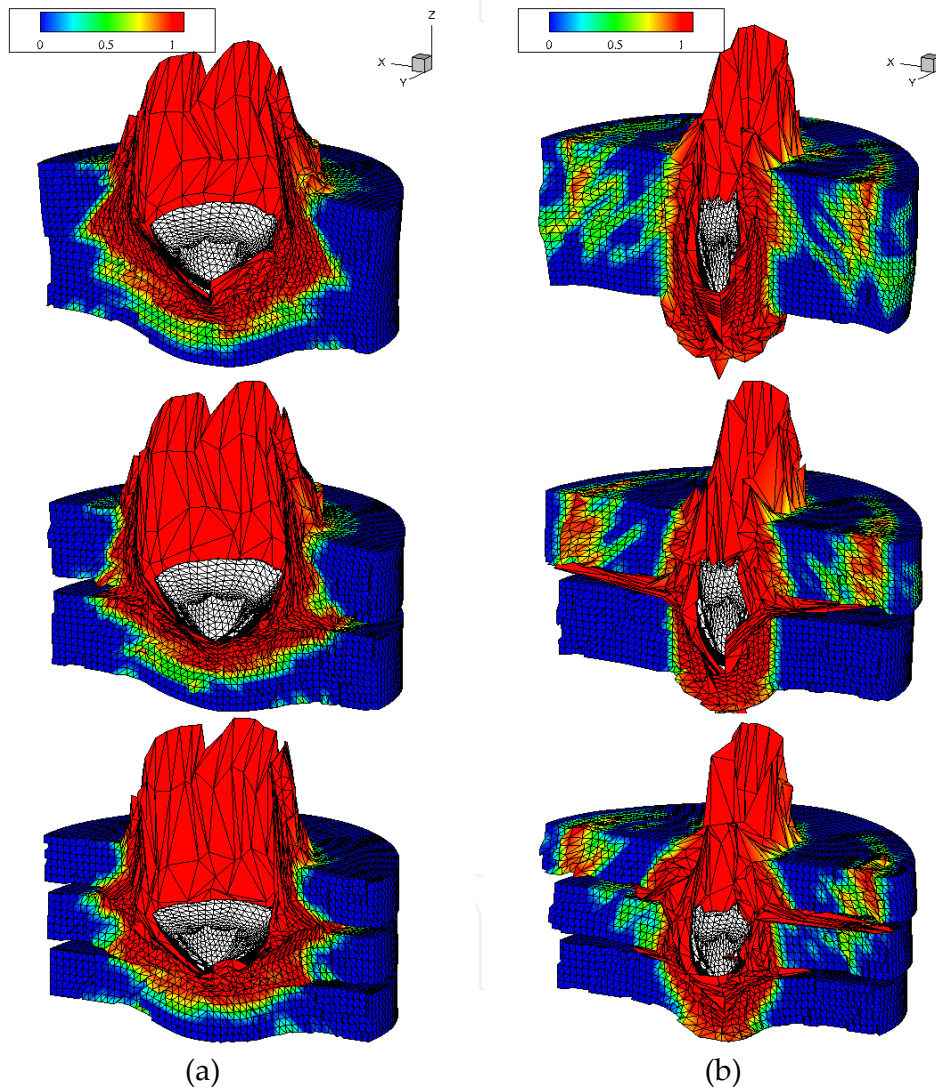


Figure 13. Calculated configurations of cooperating bodies and isolines of relative volume of fractures (V/V_0) in targets. a: $v_0 = 2000$ m/s, $\beta = 0^\circ$, b: $v_0 = 2000$ m/s, $\beta = 90^\circ$; $t = 40 \mu\text{sec}$

The fracture of barriers material begins in a compression wave ($e_{kk} \leq 0$), initiated at the moment of impact. Fracture development in barriers depends not only on value of the strength material characteristics, but also on velocities of propagation of compression and unloading waves.

In barriers made from the reoriented material (fig. 12b, fig. 13b) at the expense of greater velocity of wave propagation in an impact direction (along the axis Z) and smaller value of strength on pressure in this direction, the fracture occurring in a compression wave gets deeply on a thickness of a barrier. The unloading waves moving from free surfaces, reaching areas in which the material was already weakened at pressure, completely destroy it. In this case the projectile has before itself an extended area of the fractured material, which doesn't resist to a projectile introduction ($\sigma_{ij} = 0$).

In barriers made from an initial material (fig. 12a, fig. 13a) we have other picture: the areas of fracture realized in a compression wave, have more extended sizes in directions which are perpendicular to an impact direction. Before the projectile the area of not fractured material providing greater resistance to the projectile introduction remains.

The dynamics of fracture in barriers is estimated fully on fig. 14, which shows changes in time of the total (on a barrier) relative volume of fractures at pressure (V_p/V_0) or tension (V_t/V_0) (V_0 is total volume of barrier) for various initial velocities of impact. Curves with V_p characterize change in time of relative volume of the material destroyed in conditions of pressure ($e_{kk} \leq 0$) and keeping resistance to loading only on pressure, for monolithic and spaced (two- or three-layer) barriers. Curves with V_t characterize change in time of relative volume completely fractured material ($e_{kk} > 0$), not resisting to loading ($\sigma_{ij} = 0$). As the material fracture begins in a compression wave, at the beginning of the process volume of the fractured material being in a condition of pressure, is more than volume of the fractured material at tension. Eventually volume of the material, fractured at tension, increases at simultaneous reduction of volume of the material fractured at pressure. It is caused by influence of unloading waves, extending from free surfaces of the projectile and barriers. If for projectile velocity of 750 m/s the volume of completely fractured material ($e_{kk} > 0$) in the monolithic barrier was the smallest, with increase in impact velocity the picture changes – the volume of the fractured material in a monolithic barrier begins to exceed the corresponding values for the spaced barriers.

The comparative analysis of protective properties of the monolithic and spaced barriers made from an initial material can be spent analogically on dependences of velocity of the center of the projectile weights from time, resulted on a fig. 15 for various orientations of a material properties. For an initial orientation of a material properties at velocities of impact to 2000 m/s the more intensive braking of the projectile on a monolithic barrier occurs (fig. 15a, fig. 15b, fig. 15c). And at velocity of 750 m/s the through penetration for the monolithic and for the spaced barriers is absent. In this case during all the process of the interaction the projectile velocity falls more at interaction with the monolithic barrier. Following on efficiency is the spaced barrier made from two plates, and the least effective is a barrier made from three plates.

With increase in initial velocity of impact the picture changes. For the impact velocity of 1500 m/s the monolithic barrier is still more effective – braking of the projectile on it occurs more intensively. Post-penetration velocity of the projectile after penetration of the

monolithic barrier makes 50 m/s, after penetration of the spaced barriers – 150 m/s, but for the initial velocity of 1500 m/s in 36 μsec after the impact start the projectile velocities for cases of two-layer and three-layer spaced designs are leveled. The increase in velocity to 3000 m/s leads to that after 26 μsec after the process start the projectile begins to brake more intensively on the spaced targets, thus post-penetration velocity after penetration of the monolithic barrier is already on 10–15% above, than after penetration of the spaced barriers. For the reoriented material the tendency of increase of the spaced designs efficiency remains – with growth of velocity of interaction the difference in post-penetration velocities of the projectile after penetration of the monolithic and the spaced barriers decreases.

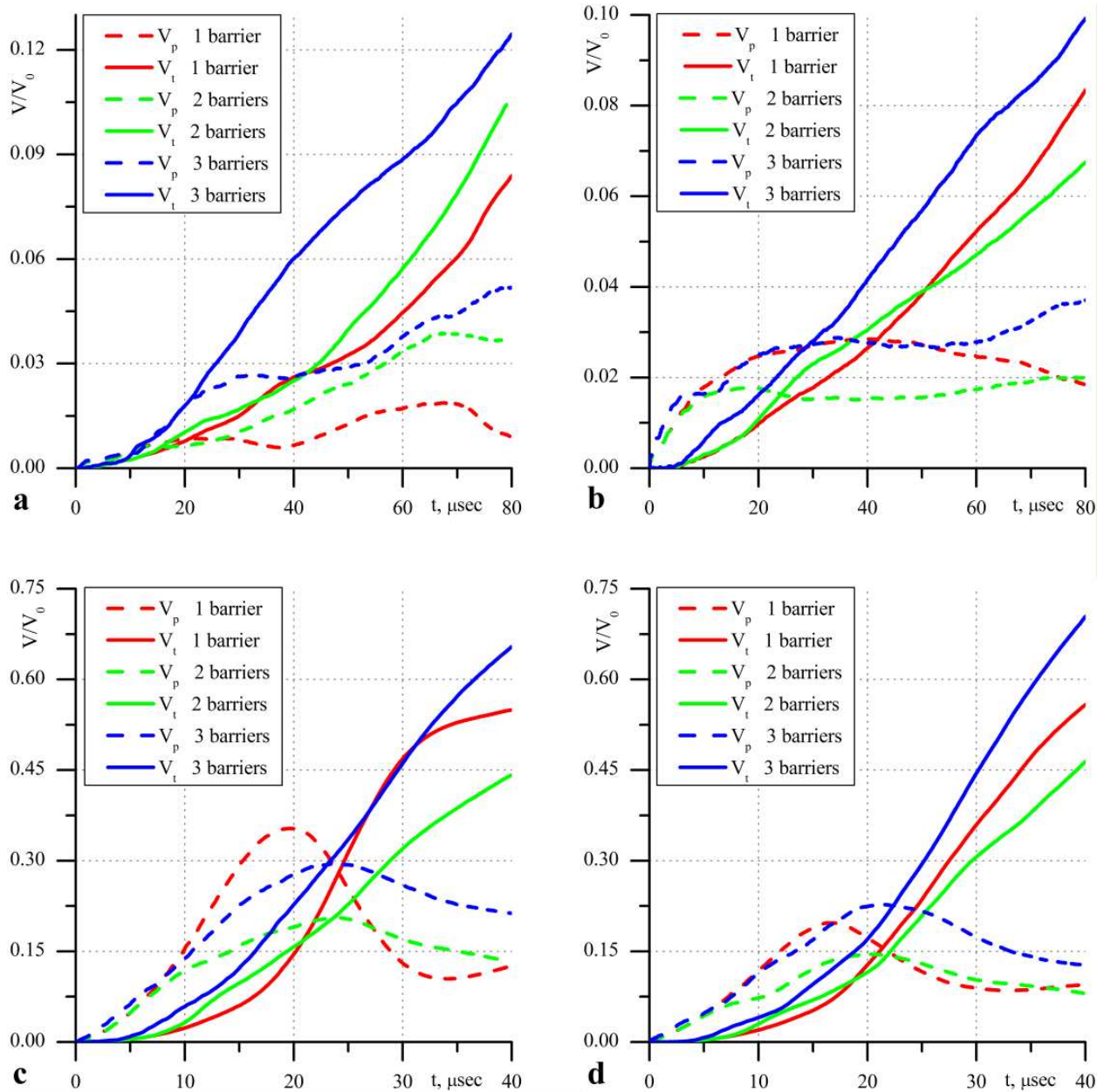


Figure 14. Relative volume of fractures at pressure and tension.

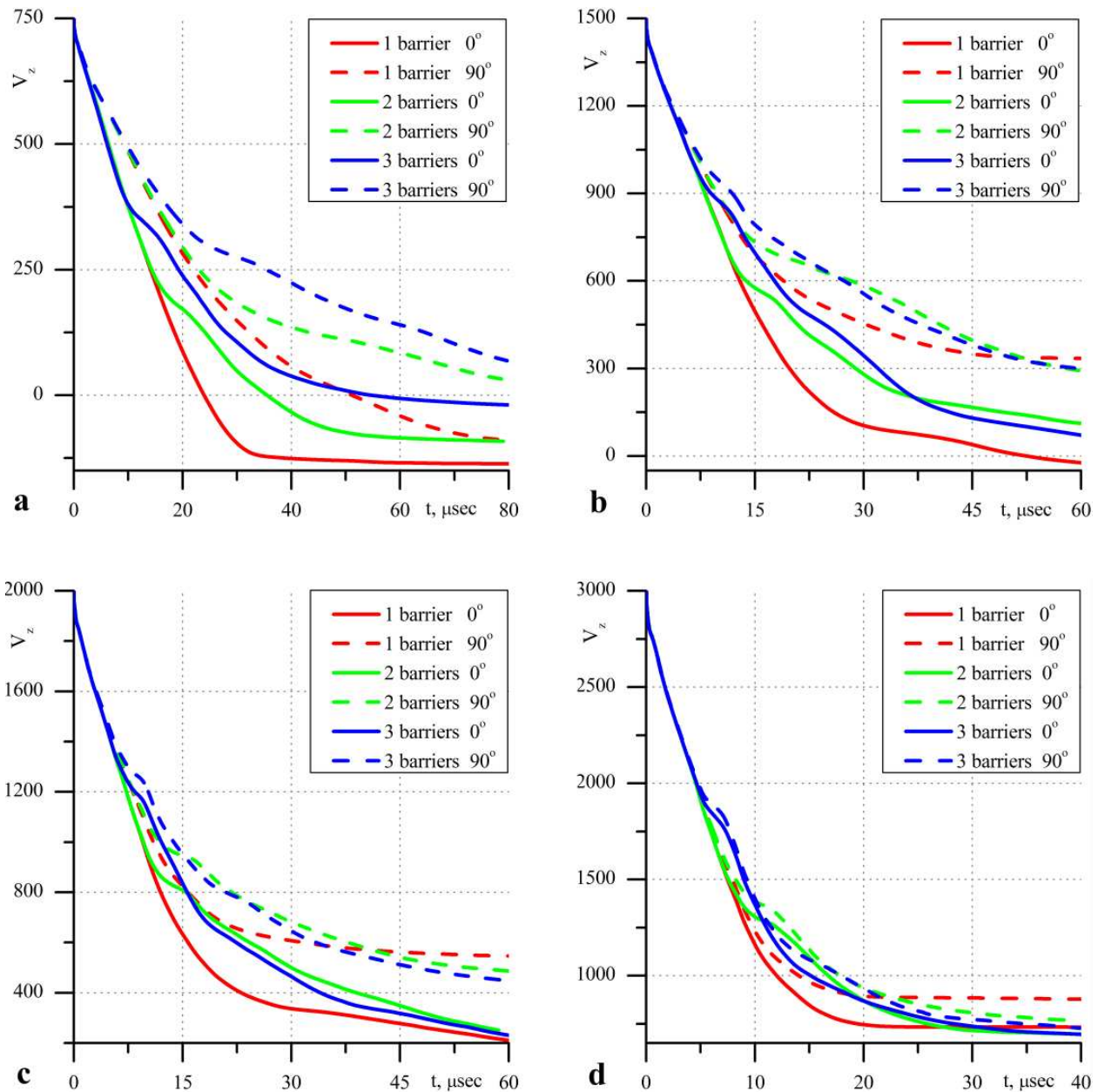


Figure 15. Velocity of the center of weights of the projectile at different initial velocities.

4.4. Numerical analysis of impact interaction of two anisotropic solids

Let's consider normal impact of orthotropic projectile with diameter 15 mm and length 75 mm and orthotropic barrier with thickness 60 mm with initial velocity $v_0 = 700$ m/c along axis Z (Radchenko & Radchenko, 2010). Orientation of properties of orthotropic material changes by turn of axes of symmetry of an initial material round an axis OY on a corner β , counted from a positive direction of an axis Z . Following cases of orientation of properties of a material of a projectile and a barrier are investigated: 0–0, 0–90, 90–0, and 90–90. Here numbers correspond to values β for a material of a projectile and a barrier in degrees, accordingly. Cases when the top and bottom half of a projectile and a barrier consist of

materials reoriented on 90° are also considered (conditionally these cases are designated as 0–90 1/2 and 45–135 1/2).

On fig. 16 settlement configurations of the projectile and a barrier and as are presented an isolines of relative volume of fracture for various cases of orientation of properties of a material. The fig. 16a corresponds to a case (0–90 1/2) when the lower half of projectile and a barrier consists of an initial material in which the greatest strength characteristics of tension are oriented in an axis direction X , perpendicular to a impact direction, and in the upper half of projectile and a barrier of property of a material are reoriented on 90° by turn concerning an axis Y . The Fig. 16b corresponds to a case (45–135 1/2) when the lower half of projectile and a barrier consist of a material in which maximum strength characteristics of tension are oriented at an angle 45° to an axis X in a plane ZX , and in the upper halves properties of a material are reoriented by turn on 90° concerning an axis Y . In the first case (Fig. 16a), besides fracture of a head part, fracture of the projectile on boundary of materials with various orientation of properties at reaching by a wave of compression of the upper half of projectile (in which the material has the minimum strength on compression in an axis direction Z), that leads to its sharing on two parts is observed. In the second case (Fig. 16b) because axes of symmetry of materials of the projectile and a barrier do not coincide with coordinate axes and, accordingly, with a direction of propagation of shock waves, fracture process in the projectile and a barrier passes not symmetrically. In the upper half of barrier the fracture area is oriented in a direction of the minimum values of strength on compression ($\beta=135^\circ$). In the projectile the fracture area as is formed on boundary of section of materials with various orientation of elastic and strength properties, but in this case fracture extends from a side surface of the projectile at an angle 135° and volume of fracture in a head part of the projectile much more.

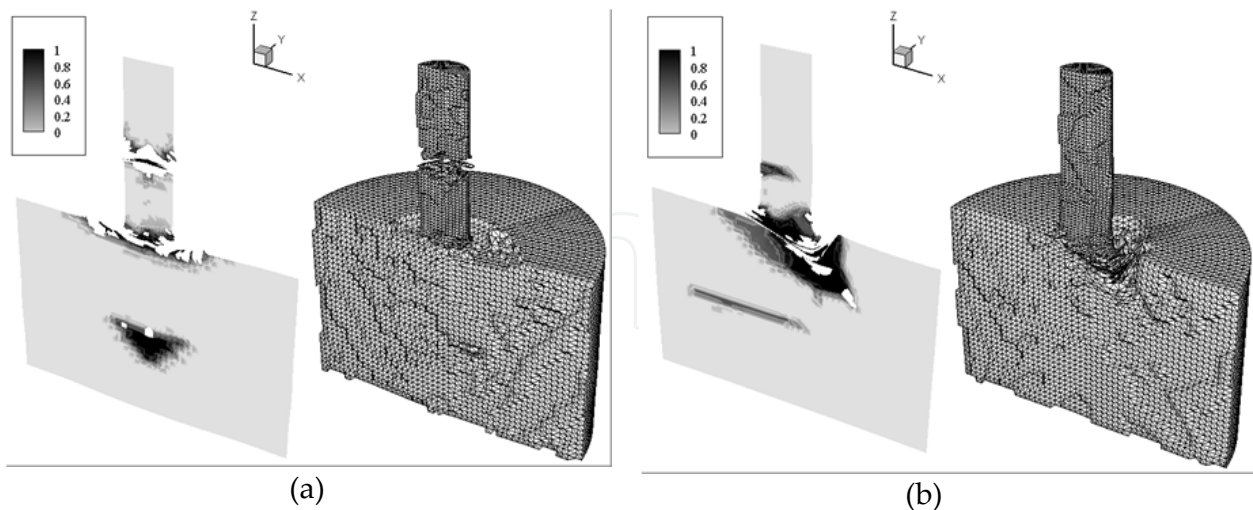


Figure 16. Configurations of interacting bodies and allocation of isolines of relative volume of fracture. $v_0 = 700$ m/s, $t = 36$ μ sec.

Dynamics of fracture in the projectile is illustrated by fig. 17 where changes in time of relative volume of the fracture derivated in the conditions of compression and tension are

resulted. The analysis of curves on Fig. 17 allows to draw a conclusion that for all considered cases of interaction the least levels of irreversible fracture (Fig. 17b) are realized in the projectile from a material with orientation of axes of symmetry $\beta = 0^\circ$. It is caused by that in this case the material of the projectile has the greatest strength properties on compression in an axis direction Z . Therefore the fracture at the initial stage of process of interaction in a wave of compression (fig. 17a), extending on length of the projectile, are minimal. For other cases of orientation of properties of a material of the projectile the volume of the fractured material in a wave of compression is more, in this connection the most part of a material of the projectile appears weakened, and further does not offer resistance at occurrence of tension powers. Curves on fig. 17a have a maximum in a range from 16 to 20 μsec , and then the volume of the material fracture at compression, decreases, after that instant the volume of irreversible fracture of a material increases at tension.

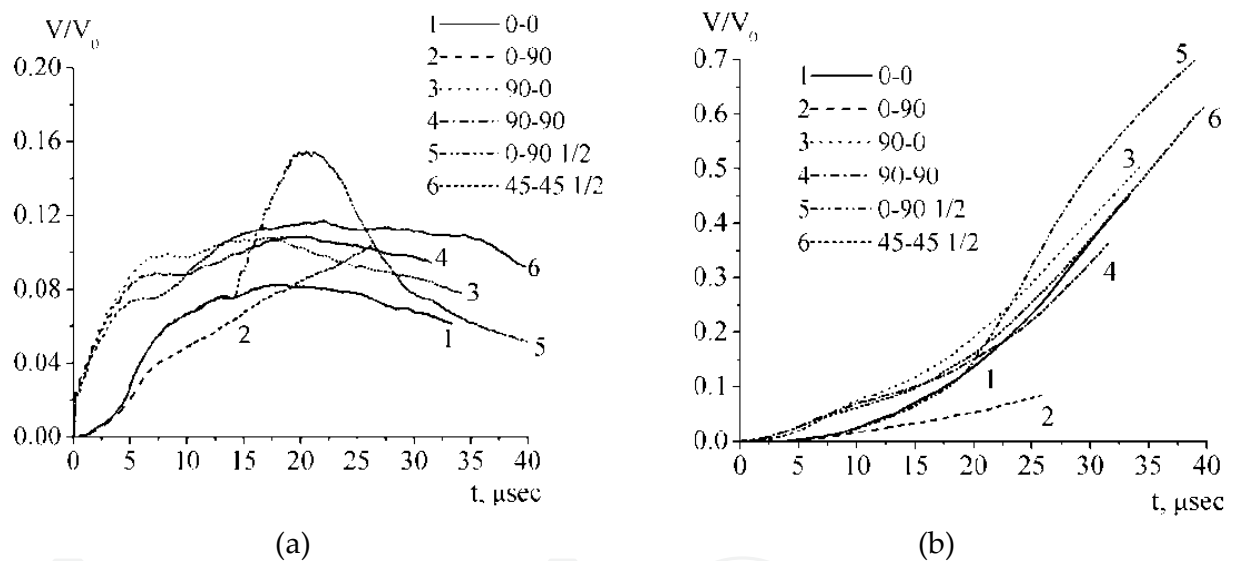


Figure 17. Change in time of relative volume of fracture in the projectile at compression (a) and tension (b) for various orientations of properties of a material.

Penetration power of the projectile depending on orientation of properties of a material at its interaction with various barriers can be estimated on the curves characterizing change in time of velocity of centre of mass the projectile (fig. 18). The most intensive braking of the projectile is observed for a case of orientation of properties 0-0 (a curve 1) and 0-90 1/2 (a curve 5). In the first of these two cases of property of a material of the projectile and a barrier are oriented equally and correspond to a case of maximum strength on compression in a direction of impact (axis Z), that stipulates high firmness of a barrier to impact. In the second case the projectile has extensive fracture and is divided on two parts (fig. 16a) that leads to loss of its penetration power.

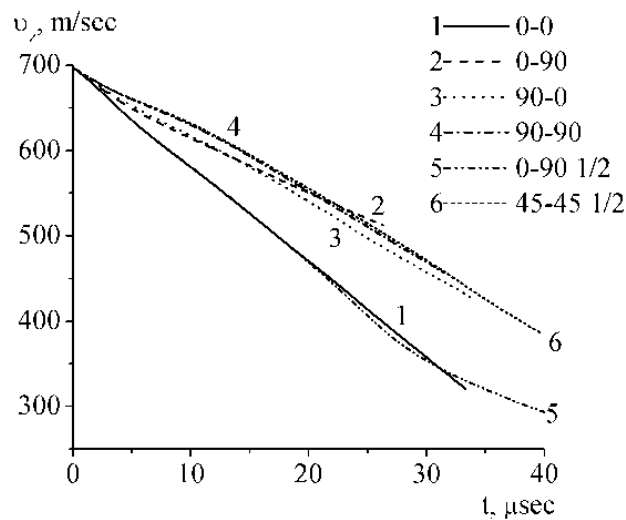


Figure 18. Change in time of velocity of centre of mass of the projectile.

5. Conclusion

1. The offered model allows to describe adequately main laws of the fracture processes of anisotropic materials under dynamic loads. The carried out researches have shown, that anisotropy of properties is the essential factor which is necessary for taking into account for the adequate description and the prediction of development of shock-wave processes and fracture in the materials under dynamic loadings. The influence of anisotropic properties orientation increases with decrease in the velocity interaction.
2. The qualitative and quantitative discrepancies in the fracture of isotropic and anisotropic materials under the dynamic loads are defined not only by strength parameters but either by the interaction of the compression and tension waves. Different velocities of waves propagation along the directions in anisotropic barriers provide the discharge of the impact wave and the narrowing in the fracture region.
3. The influence of hydrostatic pressure on the fracture of anisotropic materials under dynamic loads is shown. Full compression leads to a fragmentation of an orthotropic ball without causing the fracture of an isotropic ball. That is why adequately description of the dynamic behavior of anisotropic solids required accounting of the hydrostatic pressure.
4. It is established that at low-velocity impact formation and a direction of development of fracture zone in a target is defined by orientation of elastic and strength properties of an anisotropic material in relation to an impact direction. Depending on orientation of properties development of the conic cracks caused by combined action of tensile stresses in waves of unloading and at the expense of penetration of the projectile, or fracture of material in a pressure and unloading wave is probable.
5. A comparative analysis of the effectiveness of the protective properties of monolithic and spaced barriers from anisotropic materials for various cases of orientation of the

material properties is carried out. It is established that the effectiveness of spaced designs increases with the velocity of interaction and determined by the development of fracture in barriers, depending on the velocities of wave propagation and the orientation of the elastic and strength properties of anisotropic material with relationship to the direction of impact.

Orientation of properties of an anisotropic material of the projectile and a barrier essentially influences dynamics of fracture and on process of propagation of shock waves in the projectile and a barrier. The offered model of behavior of anisotropic materials at dynamic loads allow to carry out researches by definition of optimization of properties of a material of the projectile and a barrier at any orientation of axes of symmetry.

Author details

Andrey Radchenko

Tomsk State University of Architecture and Building, Russia

Pavel Radchenko

Institute of Strength Physics and Materials Science of SB RAS, Russia

6. References

- Ashkenazi, E. K., & Ganov, A.V. (1980) *Anisotropy of the construction materials*, Leningrad
- Johnson, G. R. Three-dimensional analysis of sliding surface during high velocity impact. (1977) *Journal of Applied Mechanics*, No. 6, pp. 771-773
- Johnson, G.R. High Velocity Impact Calculations in Three Dimension. (1977) *Journal Applied Mechanics*, Vol. 3, p. 95–100
- Kanel, G.I., Razorenov, S.V., Utkin, A.V., & Fortov, V.E. (1996) *Shock wave phenomena in condensed media*, Yanus-K, Moscow
- Radchenko, A. V., Kobenko, S.V., Marcenuk, I.N., Khorev, I.E., Kanel, G.I., & Fortov, V.E. (1999) Research on features of behaviour of isotropic and anisotropic materials under impact. *International Journal of Impact Engineering*, Vol. 23, No. 1, pp. 745–756
- Radchenko, A., Radchenko, P., Tuch, E., Krivosheina, M., & Kobenko, S. (2012) Comparison of Application of Various Strength Criteria on Modeling of Behavior of Composite Materials at Impact. *Journal of Material Science and Engineering A*, Vol. 2, No. 1, pp. 112–120
- Radchenko, A.V., & Radchenko, P.A. (2010) Numerical analysis of impact of two anisotropic solids. *Journal of Materials Science and Engineering*, Vol. 4, No. 3, pp. 74–79
- Radchenko, A.V., & Radchenko, P.A. (2011) Numerical modeling of development of fracture in anisotropic composite materials at low-velocity loading. *Journal of Materials Science*, Vol. 46, No. 8, pp. 2720–2725

Tsai, S.W., & Wu, E.M. (1971) A General Theory of Strength for Anisotropic Materials. *Journal of Composite Materials*, Vol. 5, No. 1, pp. 58–80

Wilkins, M.L., & Guinan, M.W. (1973) Impact of cylinders on a rigid boundary. *Journal of Applied Physics*, Vol. 44, No. 3, pp. 1200–1206

IntechOpen

IntechOpen